# Threshold behavior of Cu-, Ge-, Ag-$K$-, and Au-$L_3$-shell ionization cross sections by electron impact

K. Shima, T. Nakagawa, K. Umetani, and T. Mikumo
*Tandem Accelerator Center, University of Tsukuba, Ibaraki 305, Japan*
(Received 13 February 1981)

Electron-induced Cu-, Ge-, Ag-$K$ shells, and Au-$L_3$-shell ionization cross sections have been obtained from the measurement of $K\alpha$ and $L\alpha$ x-ray emission cross sections around the threshold energy. $K$- and $L_3$-shell ionization cross sections have been observed to rise as a function of $\ln(U_i)/U_i$, where $U_i$ is the ratio of electron impact energy to ionization energy. In the increasing behavior of Au-$L\alpha$ and -$L\beta$ x-ray emission cross sections with increasing impact energies, the onset of $L_2$- and $L_1$-shell ionizations have been observed at $L_2$- and $L_1$-shell ionization energies. Absolute values of Cu-, Ge-, Ag-$K$-shell ionization cross sections are well reproduced by the empirical formula of Green and Cosslett down to the vicinity of threshold energy.

## I. INTRODUCTION

The necessity has been emphasized for the measurement of electron-induced inner-shell-ionization cross sections near the threshold energies.[1,2] In fact, existing cross-section data near the threshold ($U_i < 1.2$) have been limited to $K$-shell ionizations of C ($U_K > 1.02$), N ($U_K > 1.12$), Ne ($U_K > 1.10$) by Tawara *et al.*,[3] and Ag ($U_K > 1.18$), and Au ($U_K > 1.12$) by Davis *et al.*,[4] where the reduced impact energy $U_i$ means the ratio of electron impact energy $E$ to ionization energy $E_i$ for the shell $i$. The interests of those authors were focused on the gross feature of ionization function, and less precise and detailed data points were taken around the threshold energy region.

Recently, one of the authors (K.S.) reported the Mn- and Cu-$K$-shell ionization cross sections[5] near the threshold energy, and onset behavior of cross sections were approximately reproduced by the semiempirical formula of Green and Cosslett.[6] While in outer-shell ionization it is generally accepted[7] that the onset of cross sections is proportional to $(U_i - 1)^n$ ($n$ is unity or close to unity) for single ionization, our interest is how the inner-shell-ionization cross sections behave as function of impact energy near the threshold energy. In this paper we report the $K$-shell ionization cross sections of Cu ($U_K = 1.02$–$2.8$), Ge ($U_K = 1.01$–$2.5$), Ag ($U_K = 1.02$–$1.18$) and $L_3$-shell ionization cross sections of Au ($U_{L_3} = 1.03$–$1.15$) deduced from the measurement of $K\alpha$ and $L\alpha$ x-ray emission cross sections. Particularly, the onset of cross sections less than $U_i = 1.1$ has been precisely observed.

## II. EXPERIMENT

$K$- and $L_3$-shell ionization cross sections have been deduced from $K\alpha$ and $L\alpha$ x-ray emission cross sections in impact energies between threshold and 30 keV. Experimental apparatus is shown in Fig. 1. A 30-kV dc power supply (Brandenburg 701) was used to accelerate the electrons. The area of beam spot on the target was less than 2 mm in diameter and the beam current was adjusted to be 7–80 nA in accordance with x-ray counting rate. All the incident electrons were collected by a deep Faraday cup and were led to the beam current integrator (Elcor 309C). A thin target evaporated onto a 7-$\mu$g/cm$^2$ carbon backing was placed at 45° with respect to the beam direction, and emitted x rays were detected by a Si(Li) detector positioned at 90° to the electron beam. The detector resolution was 180 eV in the value of FWHM for Mn-$K\alpha$ x rays. Some precautions especially paid are described in the following.

Firstly, accelerating voltage must be determined precisely since ionization cross sections are very sensitive to impact energy near the threshold. As shown in Fig. 1, a high resistor (490 MΩ) and a standard 10-kΩ resistor (Yokogawa 2792) were connected in series between high-voltage terminal and earth potential, and the determination of

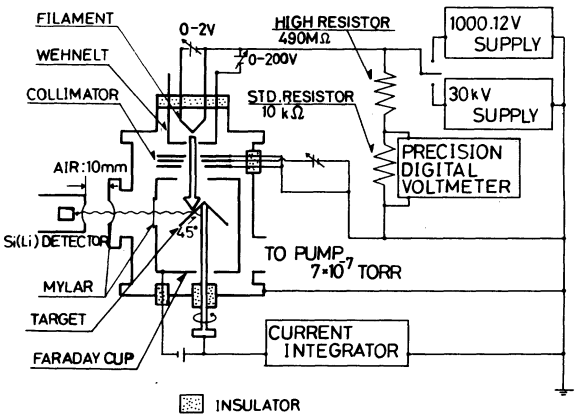


FIG. 1. Experimental arrangement.

 

high voltage was based on the reading of precision digital voltmeter (Yokogawa 2501). Just before and after the data accumulation of every run, the resistance of the high resistor was measured by switching the 30-kV supply into 3-kV supply (John Fluke 409), the output voltage of which at 1 kV was already measured to be 1000.12 V by the precision digital voltmeter. The stability of high voltage during electron beam irradiation was less than $5\times10^{-5}$, and the error in the absolute voltage is estimated to be less than 9 V.

Secondly, extremely thin and uniform targets must be used to minimize the energy loss of incident electrons. In fact, when electrons with incident energy $E_{in}$ lose energy $\Delta E$ through the passage of target layer, the mean impact energy $E$ is defined by $E_{in}-\Delta E/2$. Consequently, so long as the solid target is used, the reduced impact energy $U_i = E/E_i = (E_{in}-\Delta E/2)/E_i$ is always accompanied by the uncertainty of $\pm(\Delta E/2)/E_i$. At present, cross sections near the threshold have been measured using the targets with 4-8-$\mu$g/cm$^2$ thicknesses so as the uncertainty $(\Delta E/2)/E_i$ may not exceed the value of 0.003. Target thicknesses were measured both by the quartz-oscillator reading during evaporation and by the multiple beam interferometer. To reduce errors coming from the estimation of target thickness, standard x-ray emission cross sections have been measured for up to ten targets with different thicknesses (4–40 $\mu$g/cm$^2$) at impact energies of 25 keV for Cu-$K\alpha$, Ge-$K\alpha$, Au-$L\alpha$, and at 30 keV for Ag-$K\alpha$, where the uncertainty of cross sections caused by the broadness of $(\Delta E/2)/E_i$ becomes negligible. For repeated measurements the standard cross sections for respective x-ray emissions were found to be reproducible within error limits of $\pm 6\%$. All the data taken with the use of thin targets around the threshold have been normalized to the standard cross sections.

Thirdly, the detection efficiency of Si (Li) x-ray detector must be determined. The quantity that is necessary for the deduction of cross sections is the total detection efficiency defined by the product of (1) $\Omega/4\pi$ ($\Omega$ is the solid angle subtended by the effective area of detection), (2) detection efficiency $\epsilon$, and (3) x-ray transmission $T$ through two sheets of 9-$\mu$m windows and 10-mm air layer (see Fig. 1). For that purpose, standard radioisotopes ($^{54}$Mn, $^{57}$Co, $^{65}$Zn, $^{241}$Am, $^{137}$Cs) were placed at the target position, and x and $\gamma$ rays were detected by the Si (Li) detector. In addition, some efficiency data (Cu-, Zn-, Ge-$K$ x-ray energies) were obtained from the simultaneous measurement of electron-induced $K$ x rays by both Si (Li) and a proportional counter with known efficiency.[8] The results are shown in Fig. 2.

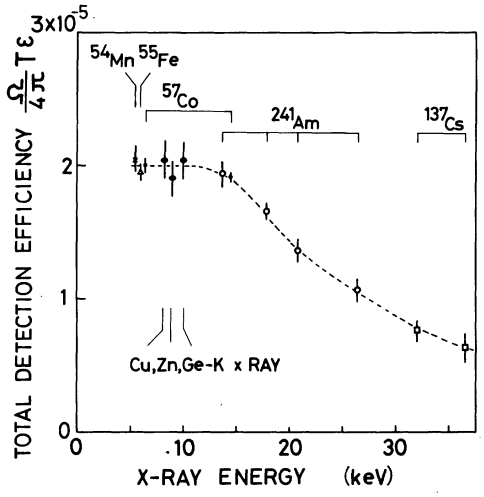


FIG. 2. Total detection efficiency of x rays as function of x-ray energy. Standard radioisotopes as well as electron-induced characteristic x rays have been used for calibration.

## III. RESULTS

Typical x-ray spectra near the threshold energy are drawn in Fig. 3 for Cu-$K$ x rays observed at the reduced impact energy of $U_K = 1.08$. The line shapes of background spectra were measured by bombarding electrons on the 7-$\mu$g/cm$^2$ carbon backing only, and were used to deduce the net x-ray peak counts.

For Cu-, Ge-, and Ag-$K$ x-ray spectra, $K\beta$ to $K\alpha$ x-ray intensity ratios $I(\beta)/I(\alpha)$ were confirmed to agree with the tabulated values by Scofield,[9] within 5%. Therefore, using Scofield's values of $I(\beta)/I(\alpha) = 0.138$ for Cu, 0.150 for Ge and 0.213 for Ag, $K$-shell ionization cross sections $\sigma_K$ have been deduced from $K\alpha$ x-ray emission

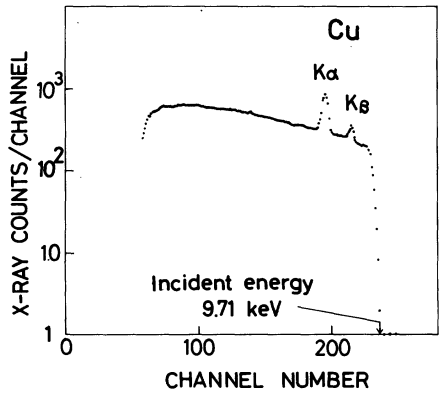


FIG. 3. Cu-$K$ x-ray spectrum observed by 9.71-keV electron irradiation.

cross sections $\sigma_{K\alpha}$ as follows:

$$\sigma_{K\alpha}=\sigma_K\omega_K\frac{I(\alpha)}{[I(\alpha)+I(\beta)]}=N_{K\alpha}\Big/\left(ndI_0\frac{\Omega}{4\pi}T_{K\alpha}\epsilon_{K\alpha}\right), \quad (1)$$

where $\omega_K$ is the $K$-shell fluorescence yield, $N_{K\alpha}$ denoting the $K\alpha$ x-ray counts, $n$ and $d$ are, respectively, target atomic density and thickness, and $I_0$ means the number of incident electrons. $\omega_K$ values for Cu, Ge, and Ag were adopted to be 0.440, 0.535, and 0.831, respectively.[10] Total detection efficiency $(\Omega/4\pi)T_{K\alpha}\epsilon_{K\alpha}$ for $K\alpha$ x rays has been taken from Fig. 2.

Au-$L_3$-shell ionization cross sections $\sigma_{L_3}$ have been deduced from $L\alpha$ x-ray emission cross sections $\sigma_{L\alpha}$. General expression of $\sigma_{L\alpha}$ is the function of $L_1$-, $L_2$-, and $L_3$-shell ionization cross sections $\sigma_{L_1}$, $\sigma_{L_2}$, $\sigma_{L_3}$, and is related to the observed $L\alpha$ x-ray counts by

$$\sigma_{L\alpha}=\frac{\Gamma_{M_{4,5}\text{-}L_3}}{\Gamma_{\text{total}\text{-}L_3}}\omega_3[\sigma_{L_3}+f_{23}\sigma_{L_2}+(f_{13}+f_{12}f_{23})\sigma_{L_1}]$$
$$=N_{L\alpha}\Big/\left(ndI_0\frac{\Omega}{4\pi}T_{L\alpha}\epsilon_{L\alpha}\right), \quad (2)$$

where $\Gamma_{M_{4,5}\text{-}L_3}$ and $\Gamma_{\text{total}\text{-}L_3}$ indicate the x-ray emission rates for $L\alpha$ ($M_{4,5}$-$L_3$ transition) and total ($M,N,O$-$L_3$ transition) x rays, respectively, $\omega_3$ the fluorescence yield for $L_3$ shell, and $f_{ij}$ means the Coster-Kronig transition probability. Isotropic distribution of $L\alpha$ x-ray emission has been assumed as is confirmed experimentally.[11] For impact energies less than $L_2$-shell ionization energy, $\sigma_{L_1}$ and $\sigma_{L_2}$ become zero and $\sigma_{L_3}$ can be directly deduced from the measurement of $\sigma_{L\alpha}$. At present, Au-$L_3$-shell ionization cross sections have been determined in this procedure for impact energies between Au-$L_3$- (11.919 keV) and -$L_2$- (13.734 keV) shell ionization energies. In addition to $\sigma_{L\alpha}$, $L\beta$ and $L\gamma$ x-ray emission cross sections $\sigma_{L\beta}$ and $\sigma_{L\gamma}$ have been measured for impact energies up to 25 keV. For gold atom, the values of 0.78 for $\Gamma$ ratio[12] in Eq. (2), and 0.32 for $\omega_3$[10] have been adopted.

In Table I, present results are listed for $K$- and $L_3$-shell ionization cross sections as well as $L\alpha$, $L\beta$, and $L\gamma$ x-ray emission cross sections. Estimated error limits added in quadrature are less than 23%. Errors mainly come from the target thickness (4–9%), net x-ray peak counts (8% around the threshold energy and 2% at higher impact energies), detection efficiency (5%) and the atomic constants used at present.

## IV. DISCUSSION

Theoretical cross sections to predict the onset behavior of inner-shell ionizations are limited. One is the classical formula by Gryzinski,[13] calculated from the binary-encounter approximation. The quantum-mechanical approach applicable to the vicinity of threshold energy is the one by Rudge and Schwartz,[14] who took into account the Born-exchange interaction by the use of the second-Born approximation. On the other hand, well-known Bethe cross sections $\sigma_i$ for the ionization of shell $i$ have the form[15] of

$$\sigma_iE_i^2U_i=6.51\times10^{-20}b_iZ_i\ln(c_iU_i)\ \text{cm}^2\text{keV}^2, \quad (3)$$

where $b_i$ and $c_i$ are Bethe parameters and $Z_i$ denotes the number of electrons in the shell $i$.

TABLE I. The measured $K$-shell ionization cross sections for Cu-, Ge-, and Ag-, $L_3$-shell ionization, $L\alpha$, $L\beta$, and $L\gamma$ x-ray emission cross sections for Au by electron impacts.

| | $E$ (keV) | $\sigma_K$ (barns) | | $E$ (keV) | $\sigma_{L_3}$ (barns) | $\sigma_{L\alpha}$ (barns) | $\sigma_{L\beta}$ (barns) | $\sigma_{L\gamma}$ (barns) |
|---|---|---|---|---|---|---|---|---|
| Cu | 9.12 | 16.1 ± 3.6 | Au | 12.26 | 45 ± 9 | 11.3 ± 1.8 | | |
| | 10.0 | 87 ± 17 | | 12.87 | 118 ± 19 | 29.6 ± 4.1 | 6.8 ± 1.6 | |
| | 15.0 | 297 ± 36 | | 13.30 | 156 ± 22 | 39.1 ± 4.7 | 9.2 ± 2.1 | |
| $\omega_K=0.440$ | 20.0 | 384 ± 41 | | 13.60 | 178 ± 25 | 44.6 ± 5.4 | 11.8 ± 2.3 | |
| | 25.0 | 401 ± 45 | | 14.70 | | 72 ± 9 | 28.7 ± 4.2 | |
| | | | $\omega_3=0.32$ | 16.00 | | 99 ± 10 | 47.0 ± 5.3 | |
| Ge | 11.20 | 4.8 ± 1.0 | $\frac{\Gamma_{M_{4,5}\text{-}L_3}}{\Gamma_{\text{total}\text{-}L_3}}=0.78$ | 17.90 | | 120 ± 12 | 72 ± 7 | 9.3 ± 2.1 |
| | 12.0 | 38 ± 6 | | 20.90 | | 150 ± 16 | 96 ± 9 | 12.2 ± 2.5 |
| | 15.0 | 139 ± 14 | | 25.00 | | 172 ± 19 | 102 ± 11 | 15.1 ± 3.0 |
| $\omega_K=0.535$ | 20.0 | 214 ± 22 | | | | | | |
| | 25.0 | 242 ± 24 | | | | | | |
| Ag | 26.0 | 1.9 ± 0.3 | | | | | | |
| | 27.0 | 6.2 ± 0.9 | | | | | | |
| | 28.0 | 9.1 ± 1.1 | | | | | | |
| $\omega_K=0.831$ | 29.0 | 12.5 ± 1.6 | | | | | | |
| | 30.0 | 16.4 ± 1.9 | | | | | | |

Since Eq. (3) is based on the first-Born approximation, its validity is limited to the region of $U_i \gg 1$. In fact, unless $c_i$ is unity, the cross section $\sigma_i$ in Eq. (3) takes nonzero value at the threshold energy. In order to link the Bethe cross sections down to the lower impact energies, several empirical formulas have been proposed. For instance, Worthington and Tomlin,[16] proposed replacing the $\ln(c_i U_i)$ term of Eq. (3) into $\ln\{4U_i/[1.65+2.35\exp(1-U_i)]\}$. In the lower impact energy region, Bethe parameters $b_i$ and $c_i$ lose their physical aspects. However, since functions of modified-Bethe cross sections in the lower impact energies still retain the similar expression with respect to the impact energy dependence, present experimental data have been plotted according to the Bethe-Fano plot.

### A. $K$-shell ionization

Cu-, Ge-, and Ag-$K$-shell ionization cross sections obtained at present are shown in Fig. 4 together with several calculated ones. Experimental cross sections are seen to rise faster than Gryzinski's classical calculation (G), which was expected to work at low impact energies. The second-Born approximation prediction including electron exchange interaction by Rudge and Schwartz (RS) is seen to fit the observed data although experimental values are systematically

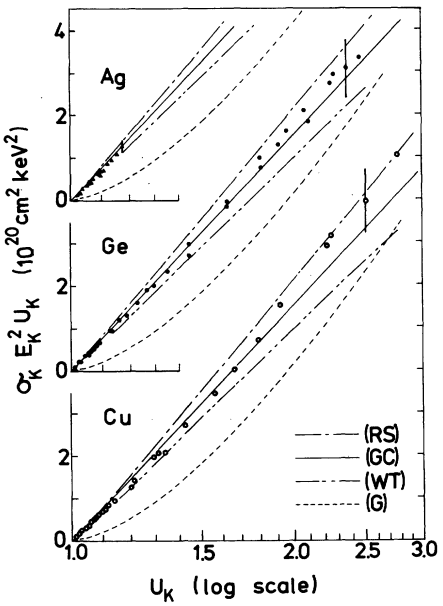


FIG. 4. Cu-, Ge-, and Ag-$K$-shell ionization cross sections in the $\sigma_K E_K^2 U_K$ vs $U_K$ representation. Theoretical and empirical cross sections are also shown: (RS) Rudge and Schwartz (Ref. 14), (GC) Green and Cosslett (Ref. 6), (WT) Worthington and Tomlin (Ref. 16), and (G) Gryzinski (Ref. 13).

lower by as much as 20% in the region of $1 < U_K < 2$. Worthington and Tomlin's semiempirical cross sections (WT) are drawn in the figure with the choice of parameter $b_i = 0.35$ since the (WT) formula was derived from Mott and Massey cross sections.[17] The attainment of agreement between observed and WT cross sections depends on the choice of parameter $b_i$. Likewise, other empirical formulas by Lotz[18] or by Drawin[19] can, in principle, fit the experimental data if only parameters are properly chosen. However, they are rather complicated functions of $U_i$ including two or three parameters.

In view of simplicity, useful empirical expression is indicated by Green and Cosslett[6] which is drawn in the figure and has the form of

$$\sigma_K E_K^2 U_K = 7.92\times10^{-20}\ln(U_k)\ \text{cm}^2\,\text{keV}^2. \quad (4)$$

The constant $7.92\times10^{-20}$ cm$^2$keV$^2$ was determined from the experiments of Ni-[20] and Ag-$K$[21]-shell ionization cross sections for region $U_K > 4$; but it is worth noting that Eq. (4) can reproduce the present Cu-, Ge-, and Ag-$K$-shell ionization data until down to almost threshold energy. In addition, the simple expression of Eq. (4) has the characteristic feature that the ratios of GC to the second-Born RS cross sections are almost constant to be 0.93–0.89 over the impact energies drawn in the figure. Since little data have been reported for inner-shell ionizations near the threshold energy, the validity of GC with regard to atomic number dependence cannot be discussed here. At least for the present intermediate atoms, GC cross sections are useful both in the absolute values and the impact energy dependence from threshold to about $U_K = 3$ where the cross sections show the broad maximum behavior.

In order to survey the threshold behavior, part of the data in Fig. 4 are again plotted in Fig. 5 in the region of $1 < U_K < 1.25$. The values of ordinate $\sigma_K E_K^2 U_K$ are seen to rise almost linearly as function of $\ln(U_K)$, taking slightly lower values than (GC) cross sections. Tentatively, this relation can be drawn by the straight line in the figure expressed by

$$\sigma_K E_K^2 U_K = 7.2\times10^{-20}\ln(U_K)\ \text{cm}^2\,\text{keV}^2. \quad (5)$$

In the outer-shell ionization of atoms with many electrons, or in the inner-shell ionization of light atoms with few electrons, the onset of a single ionization cross section is known to rise as a function of reduced excess energy $\sigma_i \propto (U_i - 1)$,[7] or to rise nonlinearly as $\sigma_i \propto (U_i - 1)^{1.127}$.[22] The former case can be calculated if one neglects the electron correlation between primary and ejected electrons, while the latter was predicted by Wannier,[22] when correlation was taken into account.

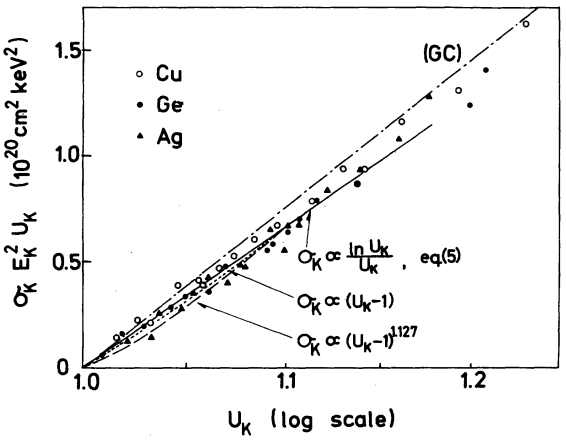


FIG. 5. Cu-, Ge-, and Ag-$K$-shell ionization cross sections near the threshold energy. Empirical cross sections by Green and Cosslett (GC) (Ref. 6) are drawn by dash dotted line. Dotted line [$\sigma_K \propto (U_K-1)$] and dashed line [$\sigma_K \propto (U_K-1)^{1.127}$] are normalized to the solid line [Eq. (5)] at $U_K=1.1$.

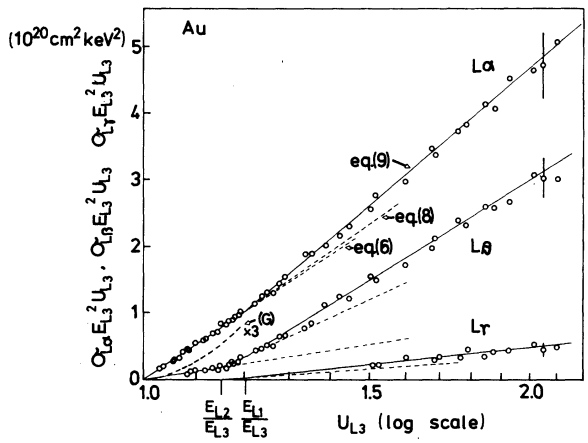


FIG. 6. Au-$L\alpha$, -$L\beta$, and -$L\gamma$ x-ray emission cross sections in the representation of $\sigma_{L\alpha}E_{L_3}^2U_{L_3}$, $\sigma_{L\beta}E_{L_3}^2U_{L_3}$, and $\sigma_{L\gamma}E_{L_3}^2U_{L_3}$ vs $U_{L_3}=E/E_{L_3}$. Solid lines indicate the evaluated values (see text) for respective impact energy region of $U_{L_3}<E_{L_2}/E_{L_3}$, $E_{L_2}/E_{L_3}<U_{L_3}<E_{L_1}/E_{L_3}$, and $E_{L_1}/E_{L_3}<U_{L_3}$, and their exterpolations are drawn by dotted lines. The prediction of $L\alpha$ x-ray emissions by Gryzinski's calculation (Ref. 6) (G) is also shown.

If we normalize the linear and nonlinear relations to Eq. (5) at $U_K=1.1$, three relations of $\ln(U_K)/U_K$, $(U_K-1)$, and $(U_K-1)^{1.127}$ come very close as are shown in Fig. 5. Although electron correlation such as exchange and interference effects is expected to become important near the threshold, neither the energy extent affected by such effects nor the change of the rising function has been predicted for the present deep inner-shell ionizations of neutral atoms. In the present observation, the choice of the proper rising function among the above-mentioned three functions is difficult since all functions fall within the scattering of data points.

### B. $L_3$-shell ionization

Observed Au-$L\alpha$, -$L\beta$, and -$L\gamma$ emission cross sections are shown in Fig. 6 as function of reduced impact energy $U_{L_3}=E/E_{L_3}$. For impact energies less than $L_2$-shell ionization energy $E_{L_2}$, linear rising behavior of $\sigma_{L\alpha}E_{L_3}^2U_{L_3}$ is seen with respect to $\ln(U_{L_3})$. With the help of Eq. (2) ($\sigma_{L\alpha}=0.25\sigma_{L_3}$ for Au), this relation can be written as

$$\sigma_{L\alpha}E_{L_3}^2U_{L_3}/0.25=\sigma_{L_3}E_{L_3}^2U_{L_3}=4C\ln(U_{L_3}), \tag{6}$$

where the value 4 stands for the number of electrons in $L_3$ shell and $C$ is the constant which is determined to be $(5.5\pm0.3)\times10^{-20}$ cm$^2$keV$^2$ as the result of least squares fitting. Equation (6) is drawn in the figure.

At impact energies greater than $L_1$- and $L_2$-shell ionization energies, experimental $\sigma_{L\alpha}$ is seen to deviate from Eq. (6) because $L_1$- and $L_2$-shell ionizations take place [see Eq. (2)]. If we assume that the constant $C$ in Eq. (6) can be commonly applied to $L_1$- and $L_2$-shell ionizations and that ionization cross sections depend only on the number of electrons occupied in the individual shell, $L_1$- and $L_2$-shell ionization cross sections $\sigma_{L_1}$ and $\sigma_{L_2}$ can be written by

$$\sigma_{L_{1,2}}E_{L_{1,2}}^2U_{L_{1,2}}=2C\ln(U_{L_{1,2}}). \tag{7}$$

With Eqs. (6) and (7) inserted into Eq. (2), $L\alpha$ x-ray emission cross sections are given by

$$\sigma_{L\alpha}E_{L_3}{}^2U_{L_3}=C\left[\left(1+\tfrac{1}{2}f_{23}\frac{E_{L_3}}{E_{L_2}}\right)\ln(U_{L_3})+\tfrac{1}{2}f_{23}\frac{E_{L_3}}{E_{L_2}}\ln\left(\frac{E_{L_3}}{E_{L_2}}\right)\right] \quad \text{for } \frac{E_{L_2}}{E_{L_3}}<U_{L_3}<\frac{E_{L_1}}{E_{L_3}}, \tag{8}$$

$$=C\left[\left(1+\tfrac{1}{2}f_{23}\frac{E_{L_3}}{E_{L_2}}+\tfrac{1}{2}(f_{13}+f_{12}f_{23})\frac{E_{L_3}}{E_{L_1}}\right)\ln(U_{L_3})+\tfrac{1}{2}f_{23}\frac{E_{L_3}}{E_{L_2}}\ln\left(\frac{E_{L_3}}{E_{L_2}}\right)+\tfrac{1}{2}(f_{13}+f_{12}f_{23})\frac{E_{L_3}}{E_{L_1}}\ln\left(\frac{E_{L_3}}{E_{L_1}}\right)\right]$$

$$\text{for } \frac{E_{L_1}}{E_{L_3}}<U_{L_3}. \tag{9}$$

Equations (8) and (9) are drawn in Fig. 6 by taking the values of 0.14, 0.53, and 0.122 for $f_{12}$, $f_{13}$, and $f_{23}$,

respectively.[10] Similarly, $L\beta$ and $L\gamma$ x-ray emission cross sections $\sigma_{L\beta}$ and $\sigma_{L\gamma}$ can be evaluated when Eqs. (6) and (7) are inserted into the formulas

$$\sigma_{L\beta}=\left(\frac{\Gamma_{N_{1,5}\text{-}L_3}+\Gamma_{O_{4,5}\text{-}L_3}}{\Gamma_{\text{total}\text{-}L_3}}\right)\omega_3[\sigma_{L_3}+f_{23}\sigma_{L_2}+(f_{13}+f_{12}f_{23})\sigma_{L_1}]+\frac{\Gamma_{M_4\text{-}L_2}}{\Gamma_{\text{total}\text{-}L_2}}\omega_2(\sigma_{L_2}+f_{12}\sigma_{L_1})+\frac{\Gamma_{M_{2,3}\text{-}L_1}}{\Gamma_{\text{total}\text{-}L_1}}\omega_1\sigma_{L_1}, \quad (10)$$

$$\sigma_{L\gamma}=\left(\frac{\Gamma_{N_{1,4}\text{-}L_2}+\Gamma_{O_4\text{-}L_2}}{\Gamma_{\text{total}\text{-}L_2}}\right)\omega_2(f_{12}\sigma_{L_1}+\sigma_{L_2})+\left(\frac{\Gamma_{N_{2,3}\text{-}L_1}+\Gamma_{O_{2,3}\text{-}L_1}}{\Gamma_{\text{total}\text{-}L_1}}\right)\omega_1\sigma_{L_1}. \quad (11)$$

Evaluated results of $\sigma_{L\beta}E^2_{L_3}U_{L_3}$ and $\sigma_{L\gamma}E^2_{L_3}U_{L_3}$ are drawn by solid lines in Fig. 6 where $\Gamma$ ratios for $L_3$, $L_2$, $L_1$ shells in Eq. (10) are 0.18, 0.79, 0.71, respectively, and those for $L_2$, $L_1$ shells in Eq. (11) are 0.19, 0.22, respectively,[12,13] and $\omega_2=0.334$, $\omega_1=0.107$.[10]

At present, the procedure to obtain the evaluated cross sections is based on the use of common constant $C$ which was experimentally determined for $L_3$-shell ionization. Quite good reproducibility of observed $\sigma_{L\alpha}$, $\sigma_{L\beta}$, and $\sigma_{L\gamma}$ by the evaluated cross sections strongly suggests the rising function of $L$-shell ionizations being approximated by $\ln(U_i)/U_i$ up to about $U_i=2$. It further suggests that the values of constant $C$ which should depend on the subshell are almost equal for at least $L_2$-, and $L_3$-shell ionizations because $L\alpha$, $L\beta$, and $L\gamma$ x-ray emissions are respectively dominated by $L_3$-, $(L_2+L_3)$-, and $L_2$-shell ionizations (see Fig. 6). The deviations of constant $C$ for $L_2$-, and $L_1$-shell ionizations from the commonly taken value can be estimated when all the observed $\sigma_{L\alpha}$, $\sigma_{L\beta}$, and $\sigma_{L\gamma}$ data are fitted by Eqs. (6) and (7) with the $C$ value for $L_3$-shell ionization fixed and other $C$ values varied. Resultant best fit can be obtained for $C=(5.4\pm0.5)$, $(5.1\pm0.9)\times10^{-20}$ cm$^2$keV$^2$ for $L_2$-, and $L_1$-shell ionizations, respectively. The trend of such subshell dependence of constant $C$ is in accordance with predictions at higher impact energies. Namely, if present empirical formulas of Eqs. (6) and (7) (valid only near the threshold) are inserted into Scofield's relativistic PWBA calculation,[24] the values of $C$ for Au-$L_3$, $L_2$, and $L_1$ shells by 50–100 keV electron impacts become (6.4–6.5), (6.2–6.3), and $(5.1–5.3)\times10^{-20}$ cm$^2$keV$^2$, respectively.

As well as $K$-shell ionizations, theoretical predictions for $L$-shell ionizations are scarce near the threshold energy. Gryzinski's cross sections[13] by classical binary-encounter approximation are drawn in Fig. 6 in the representation of $\sigma_{L\alpha}E^2_{L_3}U_{L_3}$, and show significant deviation near the threshold energy. Rudge and Schwartz[14] (RS) obtained $L_1$-shell ionization cross sections for hydrogenlike ions with the second Born and Born-exchange interaction expressed by

$$\sigma_{L_1}E^2_{L_1}U_{L_1}=3.52\times10^{-20}\left(2.168+\frac{1.147}{U_{L_1}}-\frac{0.212}{U^2_{L_1}}\right)\times\ln(U_{L_1})\text{cm}^2\,\text{keV}^2. \quad (12)$$

Although present $L_1$-shell ionization cross sections $[C=(5.1\pm0.9)\times10^{-20}$ cm$^2$keV$^2]$ are accompanied with large errors due to minor contribution of $L_1$-shell ionization to $L\alpha$, $L\beta$, and $L\gamma$ x-ray emissions, it is interesting to note that the (RS) cross sections come within the uncertainty of experimental for the present $U_{L_1}<2$ region. Extension of (RS) calculations to $L_2$ and $L_3$ shells is expected because inclusion of electron exchange effect is inevitable near the threshold energy.

## V. SUMMARY

The first and precise measurements of electron-induced inner-shell-ionization cross sections have been performed near the threshold energy. The rising function of ionization cross sections have been found to be approximated by

$$\sigma_i E_i^2 U_i = C_i Z_i \ln(U_i),$$

where $C_i$ stands for the constant depending on the shell and atom, and $Z_i$ being the number of electrons in the shell $i$. For Cu-, Ge-, and Ag-$K$-shell ionizations, Green and Cosslett's empirical expression ($C_K=3.96\times10^{-20}$ cm$^2$keV$^2$) has been found to reproduce the gross feature of ionization cross sections, but in the very near region to the threshold energy, a slight deviation (about 10% on an average) in $C_K$ value was observed. For Au-$L_3$-, -$L_2$-, and -$L_1$- shell ionizations, the values of $C_{L_3}=(5.5\pm0.3)$, $C_{L_2}=(5.4\pm0.5)$, $C_{L_1}=(5.1\pm0.9)\times10^{-20}$ cm$^2$keV$^2$ have been observed.

The accumulation of cross-section data near the threshold energy is necessary not only for the systematic interpretation of ionization process but also for the practical use such as x-ray microanalysis.

## ACKNOWLEDGMENT

We are grateful to M. Okuda and E. Suzuki for their assistance during the experiment. This work was supported in part by the Nuclear and Solid Research Project of the University of Tsukuba.

[1]C. P. Powell, Rev. Mod. Phys. 48, 33 (1976).
[2]C. A. Quarles, Phys. Rev. A 13, 1278 (1976).
[3]H. Tawara, K. G. Harrison, and F. J. de Heer, Physica (Utrecht) 63, 351 (1973).
[4]D. V. Davis, V. D. Mistry, and C. A. Quarles, Phys. Lett. A 38, 169 (1972).
[5]K. Shima, Phys. Lett. A 77, 237 (1980).
[6]M. Green and V. E. Cosslett, Proc. Phys. Soc. London 78, 1206 (1961).
[7]J. B. Hasted, *Physics of Atomic Collisions* (Butterworths, London, 1964), p. 235.
[8]K. Shima, Nucl. Instrum. Methods 165, 21 (1979).
[9]J. H. Scofield, Phys. Rev. A 9, 1041 (1974).
[10]M. O. Krause, J. Phys. Chem. Ref. Data 8, 307 (1979).
[11]J. Pálinkás, B. Schlenk, and A. Valek, J. Phys. B 12, 3273 (1979).
[12]J. H. Scofield, Phys. Rev. A 10, 1507 (1974).
[13]M. Gryzinski, Phys. Rev. A 138, 336 (1968).
[14]M. R. H. Rudge and S. B. Schwartz, Proc. Phys. Soc. London 88, 563 (1966).
[15]H. Bethe, Ann. Phys. (N.Y.) 5, 325 (1930).
[16]C. R. Worthington and S. G. Tomlin, Proc. Phys. Soc. London Ser. A 69, 401 (1956).
[17]N. F. Mott and H. S. W. Massey, in *The Theory of Atomic Collisions, 2nd ed.* (Oxford University, London, 1949), p. 243.
[18]W. Lotz, Z. Phys. 206, 205 (1967).
[19]H. W. Drawin, Z. Phys. 164, 513 (1961).
[20]L. T. Pockman, D. L. Webster, P. Kirkpatrick, and K. Harworth, Phys. Rev. 71, 330 (1947).
[21]P. Kirkpatrick and A. V. Baez, Phys. Rev. 71, 521 (1947).
[22]G. H. Wannier, Phys. Rev. 90, 817 (1953).
[23]J. H. Scofield, Phys. Rev. 179, 9 (1969).
[24]J. H. Scofield, Phys. Rev. A 18, 963 (1978).